WEAK LOCALISATION OF LIGHT BY ATOMS WITH QUANTUM INTERNAL STRUCTURE

CORD A. MÜLLER
Max-Planck-Institut für Physik komplexer Systeme
Nöthnitzer Str. 38, D – 01187 Dresden

AND

CHRISTIAN MINIATURA
Laboratoire Ondes et Désordre (FRE 2302 du CNRS)
1361, route des Lucioles, F – 06560 Valbonne

1. Introduction

1.1. WHY DO WE STUDY QUANTUM TRANSPORT?

As a commonplace, we could say that all simple problems in physics have been solved a long time ago, and that we are tempted to turn to the challenging field called, rather pompously, "wave transport in complex systems". Here, "wave" is ment to emphasize the influence of *interference* (which is truly quantum mechanical for massive particles like electrons or atoms). "Transport" implies that we are interested in situations *out of thermodynamic equilibrium* (but not too far, so that linear response theory applies). Finally, a system will be called "complex" whenever it is *disordered*, or *strongly interacting*, or *chaotic*. Our choice of this field is motivated by two aspects: on the side of applied physics, all remote sensing techniques need to incorporate the multiple scattering of waves in turbid media, and the miniaturisation process in semi-conductor industry arrives at length scales where the control of quantum interference becomes crucial. On the academic side of more fundamental physics, we would like to understand and enjoy the predictive power of the best physical theory available today: quantum theory.

The classical paradigm of transport in a disordered environment is *diffusion*. In general, a quantity $n(x,t)$ in space and time (think of a particle concentration) at equilibrium is distributed with a constant density n_0. If the quantity is locally conserved, a small variation $\delta n(x,t)$ then obeys the

diffusion equation, $(\partial_t - D_0\nabla^2)\delta n(x,t) = 0$; D_0 is the diffusion constant. Its solution in Fourier space

$$\delta\hat{n}(q,t) = \delta\hat{n}(q,0)\exp(-D_0 q^2 t) \tag{1}$$

shows that very smooth fluctuations in real space (with small wave numbers $q \to 0$) are removed on very long time scales $1/D_0q^2 \to \infty$. Indeed, because of the local conservation law, a small surplus $\delta n > 0$ cannot just simply disappear, but has to reach a place far away with a depleted density $\delta n < 0$ in order to restore the equilibrium situation $\delta n = 0$.

Classical Boltzmann diffusion theory has been used successfully to describe electric conduction in metals (first by Drude), or the diffusion of light intensity through stellar atmospheres or interstellar clouds (notably by Schuster and Chandrasekhar) [1]. However, at the microscopic level, one has to deal with waves. As an example, the quantum picture of electrons moving in a perfectly periodic crystal pinpoints the key role of interference: an electron, initially confined in a well, can resonantly tunnel through the lattice, yielding Bloch energy bands. In trying to understand the interplay between disorder and interference, P. Anderson showed that sufficiently strong disorder can suppress the quantum diffusion (leading to a vanishing diffusion constant $D = 0$), a phenomenom baptised *localisation* [2]. Later, it was realized that even far from the regime of (strong) localisation, diffusive transport is affected by interference: this so-called *weak localisation* reduces the Boltzmann diffusion constant, $D = D_0 - \delta D$, by the constructive pairwise interference of amplitudes associated with time-reversed scattering paths. Mesoscopic physics, namely the study of interference effects in wave transport through random media, was born [3].

1.2. WHY DO WE USE PHOTONS AND ATOMS?

The theory of localisation has been first developed in the condensed matter physics community. But as electrons are charged particles with a very strong and long-range Coulomb interaction, the pure one-particle picture of Anderson localisation has never been observed experimentally as far as we know. On the other hand, the radar physics community first had realized that interference of counter-propagating amplitudes can play an important role in the multiple scattering of electromagnetic waves [4]. Taking the better of the two worlds, S. John and P. Anderson suggested to study localisation using light or other non-interacting classical waves. Light scattering allows the use of modern lasers with excellent coherence properties as well as an accurate analysis of direction and polarisation. A large number of turbid media has thus been studied, from Saturn's rings to semi-conductor powders [5].

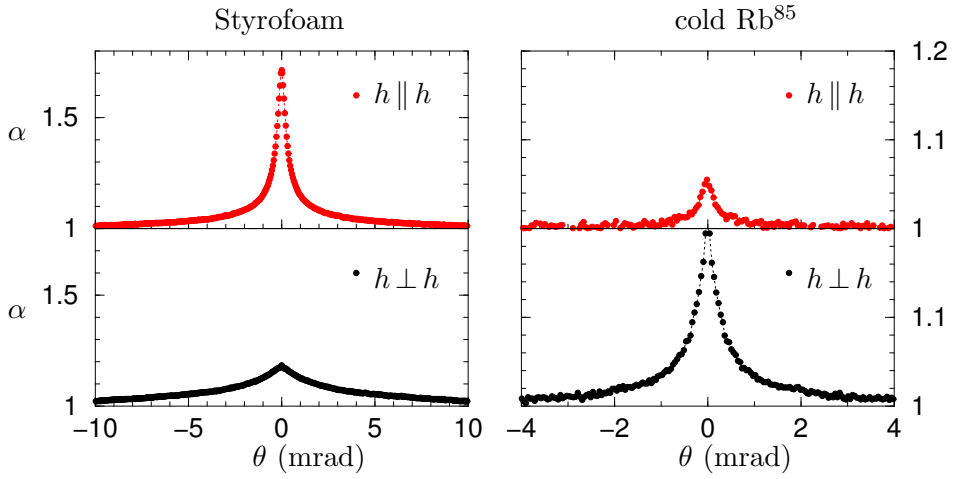

Figure 1. Experimental CBS enhancement α vs. the angle θ with respect to the backscattering direction for a classical medium (Styrofoam, left) and cold rubidium atoms (right), in the channel of preserved helicity ($h \parallel h$, top) and flipped helicity ($h \perp h$, bottom). Data generously provided by G. Labeyrie.

Today, laser-cooled atoms as light scatterers come close to a theoretician's dream team: they are perfectly identical (monodisperse) point particles. But more than that (theoretical convenience hardly ever justifies expensive experiments): their specific properties permit to study new regimes which are characterised, for example, by their quantum internal structure (as discussed in the present contribution), the finite width of the atomic fluorescence spectrum, non-linearities such as the saturation of an atomic transition, and the mechanical acceleration of the atom due to light scattering. Even more, at sufficiently low temperature, the atoms themselves become matter waves and can in turn be used to probe quantum transport, all the way down to the degenerate quantum regime of Bose-Einstein condensation (see, for example, the recent beautiful experimental realisation of the Mott-Hubbard quantum phase transition by the Munich BEC group [6]).

1.3. WHY DO WE NEED TO DESCRIBE AN INTERNAL STRUCTURE?

The first experiment of coherent backscattering of light from a cloud of cold atoms in 1999 [7, 8] yielded a surprising result (see Fig. 1): the observed interference peak in the channel of preserved helicity ($h \parallel h$) shows only a maximum enhancement of about 1.05, far below the classically expected factor of 2.0 due to reciprocity [9]. Also, this $h \parallel h$ enhancement is much

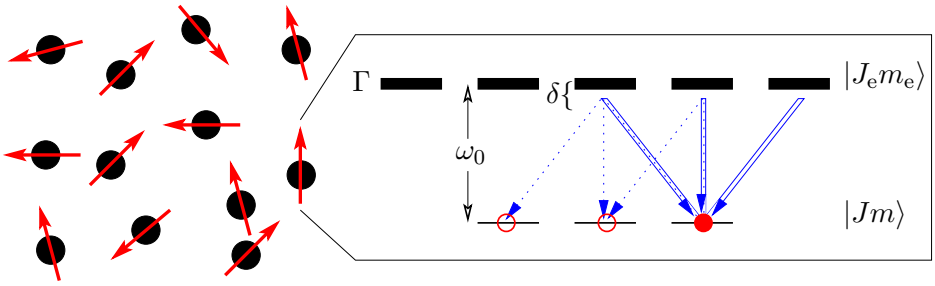

Figure 2. Left: a cloud of cold atoms as point scatterers with fixed random positions $\boldsymbol{r}$ and randomly oriented total angular momenta J. Right: a zoom into the energy level scheme of a resonant degenerate dipole transition, here the example of $J = 1$, $J_e = 2$. $\delta = \omega - \omega_0$ is the detuning of the probe light from the atomic resonance frequency ω_0, and Γ is the natural width of the excited atomic state. The polarisation of scattered polarised photons (full and dotted lines) is coupled to the internal magnetic quantum numbers m.

smaller than the measured value of 1.2 in the channel of flipped helicity ($h \perp h$). It was soon realized that the *degeneracy* of the probed atomic dipole transition $J = 3 \rightarrow J_e = 4$ is responsible for an *imbalance of CBS amplitudes* and therefore reduces the measurable enhancement factor [10]. We thus have to generalise the theory of the multiple scattering of polarised light by point dipoles to the case of an arbitrary atomic transition $J \rightarrow J_e$ [11]. This theory indeed explains the observed enhancement factors and shall be described in the following.

2. Multiple scattering of a photon by atoms with internal degeneracy

2.1. THE ONE-PHOTON TRANSITION MATRIX

Consider a cloud of laser-cooled atoms confined in a standard magneto-optical trap. The cooling is such that their velocity spread v is much smaller than the Doppler velocity Γ/k (Γ is the natural width of the excited atomic state). Therefore, we can neglect the Doppler effect and may assume that the atoms' positions $\boldsymbol{r}_\alpha, \alpha = 1, \ldots, N$, remain fixed on the light-scattering time scale. On the other hand, the velocity spread should be much larger than the recoil velocity $v_{\mathrm{rec}} = \hbar k/M$ (where M is the atomic mass) for the scattering of a photon of wave-vector k. This allows us to treat the positions as classical random variables and to follow the standard diagrammatic approach to describe multiple scattering (see [12] and references therein). The CBS probe beam with incident wave-vector $\boldsymbol{k}$, polarisation $\boldsymbol{\varepsilon}$ and frequency ω excites a closed atomic dipole transition defined by a ground state with total angular momentum J and an excited state J_e with frequency ω_0. In

the absence of a magnetic field, these two levels with internal quantum numbers m and m_e are respectively $(2J+1)$- and $(2J_\mathrm{e}+1)$-fold degenerate (see Fig. 2).

In order to minimise saturation effects and optical pumping, the experiment is performed at low laser intensity, so that we can consider the light scattering in the limit of one-photon Fock states $|\boldsymbol{k}\boldsymbol{\varepsilon}\rangle$ (in this notation, the transversality $\boldsymbol{\varepsilon}\cdot\boldsymbol{k}=0$ is understood). The transition amplitude for the scattering of an incident photon $|\boldsymbol{k}\boldsymbol{\varepsilon}\rangle$ into an emitted photon $|\boldsymbol{k}'\boldsymbol{\varepsilon}'\rangle$ by a single atom is

$$= \langle Jm'|\bar{\boldsymbol{\varepsilon}}'\cdot\boldsymbol{t}(\omega)\cdot\boldsymbol{\varepsilon}|Jm\rangle\, e^{i(\boldsymbol{k}-\boldsymbol{k}')\cdot\boldsymbol{r}}. \quad (2)$$

Note that the exponential with the classical external degrees of freedom $\boldsymbol{r}$ is factorised from the matrix element with the internal quantum numbers. Therefore, the usual multiple scattering formalism applies [12]. But we have to analyse carefully the role of the internal degrees of freedom. We see in (2) that the incident and emitted polarisation vectors $\boldsymbol{\varepsilon}$ and $\bar{\boldsymbol{\varepsilon}}'$ (the bar denotes complex conjugation) are coupled by the transition matrix $t_{ij}(m,m';\omega)=\langle Jm|t_{ij}(\omega)|Jm\rangle$. As any 3×3 matrix, it can be decomposed into its irreducible components with respect to rotations,

$$t_{ij} = \underbrace{\frac{1}{3}\delta_{ij}t_{kk}}_{t_{ij}^{(0)}} + \underbrace{\frac{1}{2}(t_{ij}-t_{ji})}_{t_{ij}^{(1)}} + \underbrace{\frac{1}{2}(t_{ij}+t_{ji})-\frac{1}{3}\delta_{ij}t_{kk}}_{t_{ij}^{(2)}} \quad (3)$$

its scalar part or trace $t^{(0)}$, its antisymmetric part $t^{(1)}$ and its traceless symmetric part $t^{(2)}$ (summation over repeated indices is understood). It is easy to verify that in the non-degenerate limit $J=0$, corresponding to the classical case of an isotropic dipole, only the scalar component $t_{ij}^{(0)}$ exists. So our task in the following will be to determine how the non-scalar components $t_{ij}^{(1,2)}$ influence the light propagation.

2.2. AVERAGE PROPAGATION INSIDE THE EFFECTIVE MEDIUM

In a disordered environment, the actual propagation depends on the precise realisation of disorder and yields, for example, an interference "fingerprint" or speckle-pattern. Universal properties can only be obtained on average. The average propagation of a light mode $|\boldsymbol{k}\boldsymbol{\varepsilon}\rangle$ inside the medium is described by the average propagator $\langle G_{ij}(\boldsymbol{k},\omega)\rangle$ where the average $\langle\ldots\rangle$ traces out the matter degrees of freedom. Following the standard procedure, we determine the average propagator in terms of the vacuum propagator

g_0 and the self-energy Σ with the aid of the Dyson equation (tensor indices are omitted for brevity)

$$\langle G\rangle = g_0 + g_0\Sigma\,\langle G\rangle = \frac{1}{g_0^{-1} - \Sigma}. \tag{4}$$

For a sufficiently dilute scattering medium such that $n\lambda^3 \ll 1$ (n is the atomic number density with typical values of 6×10^{10} cm^{-3}, and λ is the optical wavelength, typically 780 nm in the experiments done so far), the independent scattering approximation applies, and the self-energy is simply the average single-scattering t-matrix: $\Sigma_{ij}(\omega) = N\,\langle t_{ij}(\omega)\rangle$. We suppose that the atomic scatterers are *distributed uniformly* over their internal states such that rotational invariance is restored on average: $\Sigma_{ij}(\omega) = \delta_{ij}\Sigma(\omega)$. This is intuitively clear since under a scalar average only the scalar component can survive. Now, it can be checked that the scalar component is precisely the one that mimics a classical isotropic dipole:

$$\Sigma(\omega) = nM_J\frac{3\pi}{k^2}\frac{\Gamma/2}{\delta + i\Gamma/2}. \tag{5}$$

Here, the quantum internal structure only enters through the scalar factor $M_J = (2J_\mathrm{e}+1)/3(2J+1)$ with the non-degenerate limit $M_0 = 1$. The elastic mean free time is defined as $\tau = -(2\mathrm{Im}\Sigma(\omega))^{-1}$ and yields the mean free path $\ell = \tau$ in our units, where $c \equiv 1$. By virtue of the optical theorem, the mean free path is related to the total cross-section for elastic scattering by the usual Boltzmann expression $\ell = 1/n\sigma$.

Obviously, the quantum internal structure (or contribution of non-scalar components of the t-matrix) has disappeared under the scalar average over internal states, and we recover a standard scalar theory. Have we been too optimistic in hoping that the internal structure can explain the dramatic reduction of interference in the CBS signal? Well, of course not: the experimental signal in Fig. 1 is the *average intensity* which must be distinguished from the square of the average amplitude. More technically speaking, after calculating the average amplitude $\langle G\rangle$ with the Dyson equation (4), we have to turn to the average intensity $\langle \overline{G}G\rangle$.

2.3. THE AVERAGE INTENSITY VERTEX

In a dilute medium $n\lambda^3 \ll 1$, the building block for the multiple scattering series is the average single scattering intensity vertex $\langle t_{ij}\bar{t}_{kl}\rangle$ [13]. It connects two amplitudes with their respective polarisation vectors and can thus be written as a rank-four tensor,

$$\langle t_{ij}(\omega)\bar{t}_{kl}(\omega)\rangle = u(\omega)$$

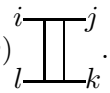

. (6)

Here, the four point polarisation vertex can be calculated analytically using standard methods of irreducible tensor operators [14]. It is simply given as the sum of the three pairwise contractions,

$$= w_1\delta_{ij}\delta_{kl} + w_2\delta_{ik}\delta_{jl} + w_3\delta_{il}\delta_{jk} \tag{7}$$

where the coefficients $w_1 = \frac{1}{3}(s_0 - s_2)$, $w_2 = \frac{1}{2}(s_2 - s_1)$ and $w_3 = \frac{1}{2}(s_2 + s_1)$ are given in terms of the squared $6J$-symbols

$$s_K = 3(2J_\mathrm{e} + 1)\left\{ \begin{array}{ccc} 1 & 1 & K \\ J & J & J_\mathrm{e} \end{array} \right\}^2 \tag{8}$$

associated with the irreducible t-matrix components $t^{(K)}$ of order $K = 0, 1, 2$. For the classical isotropic dipole $J = 0$, the coefficients become $(w_1, w_2, w_3) = (1, 0, 0)$ and yield the purely horizontal contraction $\delta_{ij}\delta_{kl}$. We see therefore that including the quantum internal structure is equivalent to replacing the simple dotted line in the usual diagrams [12] by the generalised vertex (7) with the richer topology of a *ribbon*:

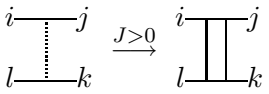

(9)

2.4. SUMMATION OF LADDER AND CROSSED SERIES

Following the standard diagrammatic approach, we have to sum the so-called series of ladder diagrams

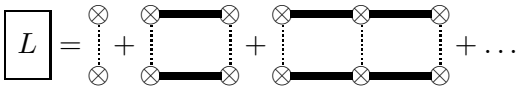

(10)

that describe the average intensity neglecting all interference terms: the direct amplitude (upper line) is scattered by the same scatterers as the conjugate amplitude (lower line), as indicated by the dotted lines. At least formally, one recognises a geometrical series that may be summed up analytically once the single scattering vertex (first term on the r.h.s.) and the square of the average propagators (thick lines) are known. The interference correction associated with CBS and weak localisation is contained in the so-called maximally crossed diagrams

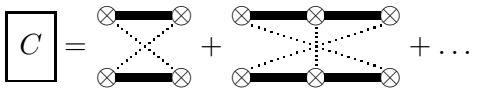

(11)

that describe the propagation of the direct and conjugate amplitude along the same scattering path, but in opposite directions. For classical point scatterers, the crossed and ladder diagrams are closely related by reciprocity: by turning around the lower line of a maximally crossed diagram, the connecting lines straighten out and yield the corresponding ladder diagram. By carefully counting incident and emitted momenta and polarisation indices, one shows that the diagrams are rigorously equal for scattering in the backward direction ($\boldsymbol{k}' = -\boldsymbol{k}$) and in the parallel polarisation channels $\bar{\boldsymbol{\varepsilon}}' = \boldsymbol{\varepsilon}$. This identity justifies the CBS enhancement factor of 2.0 in the helicity-preserving polarisation channel where, for spherically-symmetric scatterers, the single scattering contribution is absent.

In our case of a quantum internal structure, see (9), the classical vertex has to be substituted by the ribbon vertex. But now the correspondence between ladder and crossed diagrams is spoilt: when the bottom line of a crossed diagram is turned around, the connecting ribbons are twisted:

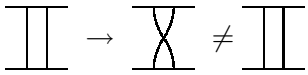

(12)

The evident difference between the twisted and the straight ribbon shows that the quantum internal structure of the atomic scatterer indeed affects the interference corrections to the average intensity. More quantitatively, twisting the vertex is equivalent to the exchange of the coefficients w_2 and w_3 associated with the diagonal and vertical contractions. Once we have calculated the ladder series, we can then obtain the crossed series by simply replacing $w_2 \leftrightarrow w_3$ (and rearranging the momenta and polarisation vectors as in the classical case).

In order to sum the geometrical ladder series, we have to determine the eigenvalues of the atomic vertex with respect to the "horizontal" direction of summation. Using a basis of projectors $\mathsf{T}^{(K)}$ onto irreducible eigenmodes $[\varepsilon_i \bar{\varepsilon}_l]^{(K)}$ of the field polarisation matrix, we obtain a decomposition of the form

$$= \sum_K \lambda_K(J, J_\mathrm{e}) \mathsf{T}^{(K)}_{il,jk} \tag{13}$$

where the eigenvalues λ_K are simple functions of the w_i:

$$\lambda_0 = 1, \qquad \lambda_1 = w_1 - w_2, \qquad \lambda_2 = w_1 + w_2. \tag{14}$$

Taking advantage of our simple substitution rule $w_2 \leftrightarrow w_3$, the twisted vertex of the crossed series then gives crossed eigenvalues χ_K such that

$$= \sum_K \chi_K(J, J_\mathrm{e}) \mathsf{T}^{(K)}_{il,jk}. \tag{15}$$

Having diagonalised the scattering vertex, we have to treat also the transverse propagation between atoms. The actual calculation is rather cumbersome because it involves momentum-dependent eigenvalues and projectors; details can be found in [15]. But our approach permits us to sum analytically the ladder and crossed series, for the full transverse vector field with arbitrary polarisation, and for arbitrary atomic transitions. It is a first step towards a generalisation of the existing multiple scattering theories, either of scalar waves by anisotropic point-scatterers [16, 17], or of vector waves by isotropic Rayleigh scatterers [18, 19].

3. Bulk transport properties

3.1. DIFFUSION AND DEPOLARISATION

The summed ladder propagator describes the average intensity distribution inside the bulk medium (*i.e.* in the absence of boundaries). To gain qualitative insight, we can simplify the exact expressions by the diffusion approximation (retaining terms of order q^2). The crucial ingredients are the atomic eigenvalues λ_K and χ_K as well as the eigenvalues $b_0 = 1$, $b_1 = \frac{1}{2}$ and $b_2 = \frac{7}{10}$ associated with the transverse propagation. The ladder propagator in the long-time limit then takes the form

$$L(q,t) = \sum_K l_K \exp\left[-D_K q^2 t - t/\tau_\mathrm{p}(K)\right]. \tag{16}$$

Apart from the factor l_K with no importance here, we first notice an exponential decay that was anticipated above in the general diffusion picture (1). We obtain the diffusion constant $D_K \approx D_0 = \ell v_\mathrm{tr}/3$ in terms of the well-known transport velocity $v_\mathrm{tr} = \ell/\tau_\mathrm{tr}$ of resonant point scatterers [12]. But there is a second exponential decay, with a characteristic polarisation relaxation time

$$\tau_\mathrm{p}(K) = \frac{\tau_\mathrm{tr}}{1/b_K\lambda_K - 1}. \tag{17}$$

The scalar field mode ($K = 0$) describes the total intensity. Its relaxation time is infinite ($\tau_\mathrm{p}(0) = \infty$) for all atomic transitions (since $b_0 = \lambda_0 = 1$), and we recover a purely diffusive behaviour as required by energy conservation. The non-scalar field modes are exponentially damped on finite, and

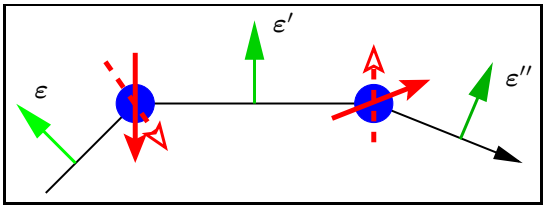

Figure 3. The transversality of propagation depolarises the multiply scattered light. This depolarisation is enhanced by an atomic quantum internal structure $J > 0$ (as discussed in sec. 3.1). Furthermore, the internal degeneracy leads to dephasing of the interference correction (as discussed in sec. 3.2).

in fact rather short time scales $\tau_{\rm p}(1,2) \leq \tau_{\rm tr}$: this simply says that a well-defined field polarisation is scrambled in the course of multiple scattering. With increasing degeneracy $J > 0$ of the atomic transition, these times get even shorter ($\lambda_K < 1$), which nicely confirms the intuitive picture that random transitions between different atomic Zeeman substates enhance the depolarisation.

3.2. WEAK LOCALISATION AND STRONG DEPHASING

Under the same approximations, the sum of crossed diagrams yields a contribution

$$C(q_c, t) = \sum_K c_K \exp\left[-D_K q_c^2 t - t/\tau_{\rm p}(K) - t/\tau_\phi(K)\right] \tag{18}$$

as a function of the total momentum $q_c = ||\boldsymbol{k} + \boldsymbol{k}'||$. One first recognises the same exponential decay as in the ladder contribution (17), indicating that depolarisation also affects the coherent contribution. But there is an additional source of exponential damping described by dephasing times [20]

$$\tau_\phi(K) = \frac{b_K \tau_{\rm tr}}{1/\chi_K - 1/\lambda_K} \tag{19}$$

which we define precisely as the damping times *with respect to* the incoherent depolarisation times. Of particular interest is the dephasing time $\tau_\phi(0)$ of the scalar mode or intensity. For atomic transitions of the type $J_{\rm e} = J + 1$, we find explicitly

$$\tau_\phi(0) = \frac{\tau_{\rm tr}}{J(2J+3)}. \tag{20}$$

The interference is only preserved ($\tau_\phi = \infty$) for classical dipoles $J = 0$. For the least possible degeneracy $J = \frac{1}{2}$, the dephasing time is already as

short as $\tau_{\rm tr}/2$ and decreases as $1/J^2$. Even if the exact expression becomes meaningless for larger J (since the diffusion approximation is certainly not justified on time scales shorter than the transport time), it is evident that the internal structure destroys the interference very effectively. Therefore, in the presence of a quantum internal structure, we only expect a (very, very) weak localisation correction to the Boltzmann diffusion constant of light propagation.

4. Coherent backscattering

We wish to calculate the CBS peak [21] analytically for arbitrary atomic transitions and therefore choose the simplest possible geometry of the scattering medium, a semi-infinite half-space. Having calculated the bulk propagator $F_0(\boldsymbol{r}_1-\boldsymbol{r}_2)$ (either the ladder or the crossed contribution), we define the corresponding propagator for the semi-infinite half space by using the method of images, $F(\boldsymbol{r}_1,\boldsymbol{r}_2) = F_0(\boldsymbol{r}_1-\boldsymbol{r}_2) - F_0(\boldsymbol{r}_1-\boldsymbol{r}_{2'})$. The image point $2'$ is defined with respect to a mirror plane lying at a distance z_0 outside the boundary of the medium. Following the habits of the field, we use the so-called "skin layer depth" $z_0 \approx 0.7121\,\ell$ pertaining to the exact solution of the homogeneous Milne equation for vector waves and point dipole scatterers [18, 19].

By this approach, we can calculate the CBS enhancement factors and peak shapes *beyond the diffusion approximation* (which is crucial whenever only short paths contribute). The CBS enhancement factor α is plotted in Fig. 4 as a function of J for transitions of the type $J \to J+1$. In the classical limit $J = 0$, we recover values of $\alpha = 2.00$, 1.76, 1.24 and 1.12 for the different polarisation channels which are in excellent agreement with the exact values obtained by a solution of the vector Milne equation by the Wiener-Hopf method [18, 19]. This indicates that the method of images can be used with success even for signals involving short scattering paths (like in the perpendicular channels) provided that the *exact* propagator (beyond the diffusion approximation) be used.

Figure 4 shows that the least internal degeneracy reduces the CBS interference dramatically: the perfect factor of 2.0 in the $h \parallel h$ channel plunges down to 1.04, well below the other three polarisation channels. At this point, our theory indeed explains the astonishing experimental result shown in Fig. 1 that has motivated this work. Furthermore, an experiment using cold Strontium atoms without internal degeneracy ($J = 0$) has recently confirmed that excellent enhancement factors in agreement with the theoretical predictions are obtained [22].

Figure 5 shows a comparison between calculated CBS peak shapes for isotropic point scatterers (left side) and atoms with $J = 3 \to J_{\rm e} = 4$

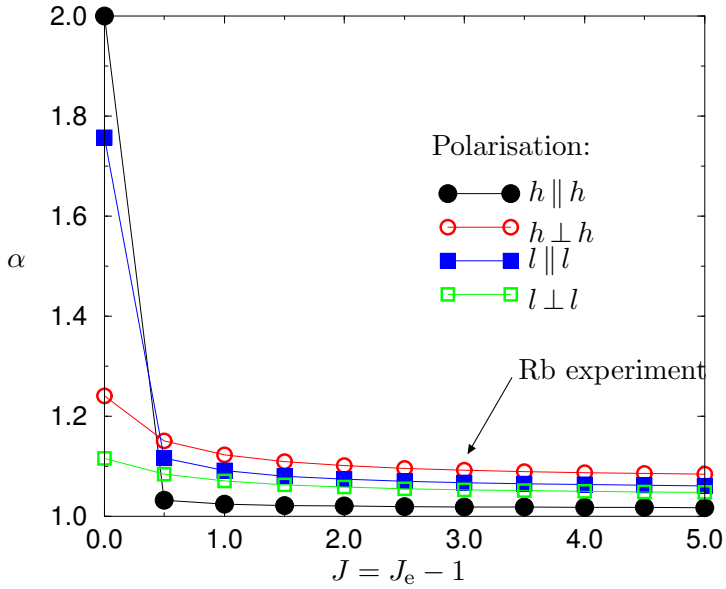

Figure 4. Calculated CBS enhancement factors at exact backscattering from a homogeneous half-space of atoms with a degenerate dipole transition $J \to J+1$ for the four usual channels of preserved ($\parallel$) and flipped ($\perp$) linear polarisation (l) or helicity (h). Contrary to the classical case, for atoms with $J > 0$ the best enhancement is expected in the $h \perp h$ channel.

(right side). The full lines are the sum of all scattering orders, and the dotted lines indicate the double scattering contribution (which is known in closed form [14]). Whereas the CBS peak in the classical case and parallel polarisation channels contains very high orders of scattering (corresponding to long scattering paths), the atomic internal degeneracy cuts off these contributions (as indicated already by the dephasing times (19)) and yields only very small peaks.

A quantitative comparison of the theory to the experimental results needs to take into account the finite geometry of the actual atomic cloud (roughly spherical, with a Gaussian density distribution). This means that analytical results are out of reach, and a numerical approach has to be taken. A Monte Carlo simulation of photon trajectories in various geometries has been realized by D. Delande and yields results which are in good agreement with the experimental data [23].

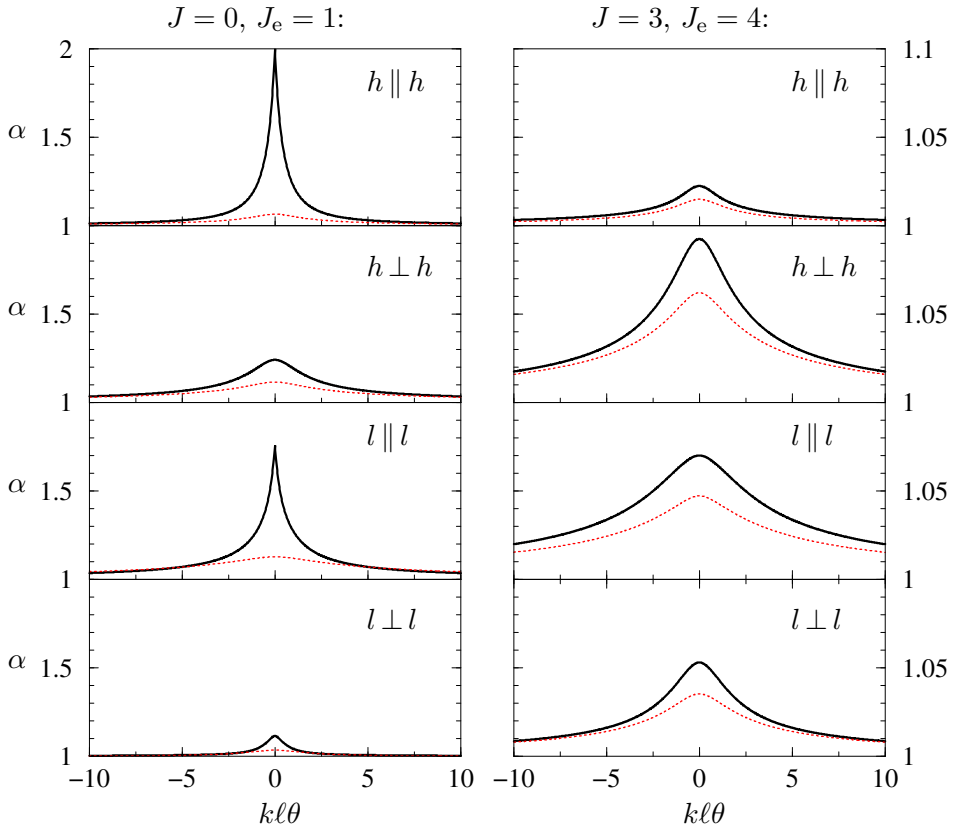

Figure 5. Calculated CBS enhancement factor α as a function of the reduced backscattering angle $k\ell\theta$ for isotropic dipole scatterer (left) and atoms with a degenerate $J = 3 \rightarrow J_e = 4$ transition (right). Full line: sum of all scattering orders. Dotted line: double scattering contribution.

5. Concluding remarks and acknowledgements

In summary, we have presented an analytical theory of the multiple scattering of polarised photons by resonant atomic dipole transitions with arbitrary degeneracy. We have shown how the usual diagrammatic approach can be generalised by using an intensity vertex with a "ribbon" topology that breaks the equivalence of ladder and crossed diagrams. The theoretical CBS peak heights reproduce the experimental results: the quantum internal structure indeed reduces the CBS interference drastically. Inasmuch as weak localisation acts as a precursor for Anderson localisation, our results indicate that in order to reach the strong localisation regime with cold atoms, the use of a non-degenerate transition is highly recommendable.

We hope to have demonstrated that atoms are light scatterers with intriguing interference properties. They permit to set up a microscopic theory for diffusion and weak localisation and thus promise to be a source of further inspiration for both fields of "disordered systems/multiple scattering" and "atomic physics/quantum optics".

It is a pleasure to acknowledge the invaluable help by Dominique Delande (who is to be credited for the "exact-image" method), many inspiring discussions with Eric Akkermans (who is to be credited for the "dephasing" interpretation), and a critical reading of the manuscript by Andreas Buchleitner.

References

1. Drude P, Annal. d. Phys. **1**, 566 (1900); Schuster A, Astrophys. J. **21**, 1 (1905); Chandrasekhar S, *Radiative Transfer* (Dover, New York, 1960)
2. Anderson P W, Phys. Rev. **109**, 1492 (1958)
3. *Mesoscopic quantum physics*, Les Houches session LXI, E. Akkermans, G. Montambaux, J.L. Pichard and J. Zinn-Justin editors, North-Holland (1995)
4. Watson K M, J. Math. Phys. **10**, 688 (1969)
5. Mishchenko M, Astrophys. J. **411**, 351 (1993); Wiersma D et al., Phys. Rev. Lett. **74**, 4193 (1995)
6. Greiner M, Mandel O, Esslinger T, Hänsch T W and Bloch I, Nature **415**, 39 (2002)
7. Labeyrie G, de Tomasi F, Bernard J-C, Müller C A, Miniatura C and Kaiser R, Phys. Rev. Lett. **83**, 5266 (1999)
8. Labeyrie G, Müller C A, Wiersma D S, Miniatura C and Kaiser R, J. Opt. B: Quant. Semiclass. Opt. **2**, 672-685 (2000)
9. B.A. van Tiggelen and R. Maynard, in *Wave Propagation in Complex media*, IMA Vol. 96, edited by G. Papanicolaou (Springer, New York, 1997), 252
10. Jonckheere T, Müller C A, Kaiser R, Miniatura C and Delande D, Phys. Rev. Lett. **85**, 4269 (2000)
11. Müller C A, PhD thesis (Universities of Munich/Nice – Sophia Antipolis, 2001), `http://www.ub.uni-muenchen.de/elektronische_dissertationen/physik/Mueller_Cord.pdf`
12. van Rossum M C W and Nieuwenhuizen T M, Rev. Mod. Phys. **70**, 313 (1999)
13. Lagendijk A and van Tiggelen B A, Phys. Rep. **270**, 143 (1996)
14. Müller C A, Jonckheere T, Miniatura C and Delande D, Phys. Rev. A **64**, 053804 (2001)
15. Müller C A and Miniatura C, J. Phys. A: Math. Gen. **35** (2002) 10163-10188
16. Ozrin V D, Phys. Lett. A **162** 341 (1992)
17. Amic E, Luck J M and Nieuwenhuizen T, J. Phys. A: Math. Gen. **29**, 4915 (1996)
18. Ozrin V D, Waves Rand. Media **2** 141 (1992)
19. Amic E, Luck J and Nieuwenhuizen T, J. Phys. I France **7** 445 (1997)
20. Akkermans E, Miniatura C and Müller C A, in preparation, `cond-mat/0206298`
21. Akkermans E, Wolf P and Maynard R, J. Phys. Fr. **49**, 77 (1988); van der Mark M, van Albada M and Lagendijk A, Phys. Rev. B **37**, 3575 (1988)
22. Bidel Y, Klappauf B, Bernard J-C, Delande D, Labeyrie G, Miniatura C, Wilkowski D and Kaiser R, Phys. Rev. Lett. **88** 203902 (2002)
23. Labeyrie G, Delande D, Müller C A, Miniatura C and Kaiser R, Europhys. Lett. **61**, 327 (2003)